INORGANIC CHEMISTRY FRONTIERS

RESEARCH ARTICLE

View Article Online
View Journal | View Issue

Cite this: *Inorg. Chem. Front.*, 2023, **10**, 2618

Carboxylate engineering for manipulating the optical and assembly properties of copper clusters†

Jing Sun,‡[a,b] Fang Sun,‡[e] Jiaqi Tang,‡[c] Xiongkai Tang,‡[d] Qingyuan Wu,[d] Rong Huo,[a] Ayisha He,[a] Sachurilatu,[a] Xueli Sun,[a] Chaolumen,*[b] Qing Tang *[e] and Hui Shen *[a]

Received 5th March 2023,
Accepted 22nd March 2023

DOI: 10.1039/d3qi00409k

rsc.li/frontiers-inorganic

Surface ligands are critical in the construction and stabilization of atomically precise metal nanoclusters (NCs) with diverse structures, and ligand engineering remains one of the most effective ways to tailor their properties. In this work, we report the synthesis, structure and surface engineering of novel copper nanoclusters co-protected by carboxylic and thioate ligands. The two clusters share the same formula $Cu_{14}(RCOO)_6(AdmS)_8$ (RCOOH is benzoic acid or 2-[(2,6-dichlorophenyl) amino] benzeneacetic acid, and AdmSH is 1-adamantanethiol) and a similar molecular structure. What is surprising to us, however, is that the optical properties, stability and assembly structures of the two clusters are significantly different, thus strongly indicating the potential of engineering carboxylates for manipulating the physicochemical properties of atomically precise copper NCs. This work not only provides model clusters stabilized by carboxylic ligands for further study of the structure–property relationship, but also outlines the big picture of carboxylic-stabilized metal nanoclusters that will flourish in the near future.

Introduction

Owing to ultra-small sizes, well-defined structures, and unique electronic structures, atomically precise metal nanoclusters (NCs) have attracted widespread interest across the fields of bio-imaging, chemical sensing, catalysis, and nanomedicine.[1–7] The clusters with precise structures are model platforms to explore the relationship between structures and properties at the atomic level, and thus direct the synthesis of functional nanomaterials for target applications in a reasonable way.[8–16] In particular, the properties of metal NCs heavily rely on their compositions, charges and structures, in which the metal–ligand interface is crucial. It has been well documented that electronic structures, local coordination environments, and physicochemical properties are susceptible to delicate changes of ligand–metal interfacial structures.[17–25] Therefore, it is of significance to deepen the understanding of the correlation between interfacial structures and physicochemical properties of metal NCs.[19,22,23,26] In the past decades, great effort was made in engineering ligands for the construction and stabilization of atomically precise metal NCs with diverse interfacial structures, which are represented by metal-phosphine, metal-thiol, metal-alkynyl, metal-halide, and metal-N-heterocyclic carbene.[6,11,15,19–21,23,24,27–45]

Close examination of the literature reveals that although significant advancements have been made in illustrating the interfaces of metal NCs by introducing diverse ligands, much less explored in the community are carboxylates. Due to their great affordability, availability, and variety, carboxylate ligands have evolved to be some of the most common compounds that find wide application in the fields of organometallics, materials, catalysis, *etc.*[18,46–59] Of note, the presence of carboxylate ligands on the surface of a handful of metal NCs is a pioneering implication for tailoring physicochemical properties of metal NCs by engineering carboxylate groups.[60–62] Recently, several important studies have clearly demonstrated that carboxylates have emerged as a new class of ligands in the field of NCs. It has even been claimed from the viewpoint of theoretical calculations that carboxylates would enable great tunability of geometric structures, hence making them attractive

[a]*College of Energy Materials and Chemistry, Inner Mongolia University, Hohhot 010021, China. E-mail: shen@imu.edu.cn*
[b]*College of Chemistry and Chemical Engineering, Inner Mongolia University, Hohhot 010021, China. E-mail: chaolumen@imu.edu.cn*
[c]*CAS Center for Excellence in Nanoscience, Beijing Key Laboratory of Micro-nano Energy and Sensor, Beijing Institute of Nanoenergy and Nanosystems, Chinese Academy of Sciences, Beijing, 101400, China*
[d]*State Key Laboratory of Physical Chemistry of Solid Surfaces and College of Chemistry and Chemical Engineering, Xiamen University, Xiamen, 361005, China*
[e]*School of Chemistry and Chemical Engineering, Chongqing Key Laboratory of Theoretical and Computational Chemistry Chongqing University, Chongqing, 401331, China. E-mail: qingtang@cqu.edu.cn*

†Electronic supplementary information (ESI) available. CCDC 2216708 and 2216705. For ESI and crystallographic data in CIF or other electronic format see DOI: https://doi.org/10.1039/d3qi00409k

‡These authors contributed equally to this work.

ligands for endowing NCs with interesting catalytic, photocatalytic, and optical properties.[63] Experimentally, the reports by Liu and co-workers for determining the crystal structure of all-carboxylate protected superatomic Ag_8 for the first time, and by Wang and co-workers for preparing amino carboxylate-stabilized Ag_{47} with homochirality have clearly illustrated that carboxylate-stabilized NCs feature interesting optical properties, thus providing us a bright prospect for further functionalizations.[64,65]

Although carboxylate ligands have been introduced in the protection of metal NCs in previous reports, engineering carboxylate ligands for manipulating the optical and assembly properties of metal NCs such as copper, to the best of our knowledge, has not been claimed. Herein, we report the synthesis and structural determinations of two novel copper clusters co-stabilized by carboxylate and thiol ligands: $[Cu_{14}(BEN)_6(AdmS)_8]$ (Cu_{14}-1) and $[Cu_{14}(diclofenac)_6(AdmS)_8]$ (Cu_{14}-2) (BEN is benzoic acid, diclofenac is 2-[(2,6-dichlorophenyl) amino] benzeneacetic acid, and AdmSH is 1-adamantanethiol). Although the two Cu_{14} clusters share similar formulas, charges and structures, the use of different carboxylate ligands induces significant changes in their optical, stability and assembly properties, which therefore indicates the bright future of engineering carboxylate ligands for regulating the properties of NCs.

Results and discussion

The two Cu_{14} clusters were prepared by the hydrothermal reduction method reported by Melosh *et al.*[66] $Cu(RCOO)_2$ salts were reduced by ethylene glycol under thermal treatment in the presence of thiols to afford raw products (see the Experimental section for details). Bright yellow crystals suitable for single crystal X-ray diffraction analysis were obtained by vapor diffusion of ether into the cluster solution (Fig. S1 and S2†).

Structural analysis revealed that Cu_{14}-1 crystallized in a triclinic system with a space group of $P\bar{1}$, and Cu_{14}-2 in a monoclinic unit cell in the $P2_1c$ space group (Tables S1 and S2†). Due to the structural similarity of these two nanoclusters, we here present only the detailed structure of Cu_{14}-1. The asymmetric unit in the structure of Cu_{14}-1 contains 156 crystallographically independent sites, *i.e.*, fourteen Cu, eight AdmSH ligands and six BEN ligands. In addition, no counterion was observed in the lattice, which indicates that it is a neutral molecule. Thus, the empirical formula of Cu_{14}-1 was proposed to be $[Cu_{14}(BEN)_6(Adms)_8]$ (Fig. S3 and S4†). On the basis of its formula, all the 14 copper atoms are in the +1 oxidation state, which suggests the effective reduction of Cu^{2+} by ethylene glycol under heating conditions.

The metal skeleton of Cu_{14}-1 was simultaneously protected by different types of donors of hard Lewis groups of O and the soft Lewis ones of S (Fig. 1a). The structure features a $Cu_{12}S_8$ core which could be viewed as two S atoms tetrahedrally embedded in the Cu_{12} framework (Fig. 1b). Considering the monovalent valence state of copper ions, the metal framework of Cu_{14}-1 has an excessively positive charge. In order to make the structure stable, the core of Cu_{14}-1 was further passivated by six BEN ligands that are less sterically demanding to form isolated neutral clusters. The metal framework of the cluster can be regarded as a malformed prismatic structure consisting of four prongs, and the thiol ligands act as bridging units to connect the four prongs to each other (Fig. 1c). Besides, the two Cu atoms at the end positions of each prong are capped by BEN ligands with Cu–O bond lengths of 1.863–2.044 Å (Fig. 1d), which is consistent with the literature reports.[67]

Compared with previously reported copper clusters capped by thiolate ligands, the introduction of BEN ligands not only makes the entire structure of Cu_{14}-1 distinct, but also brings great significance for the construction of new connection patterns within the clusters. For example, the structure of Cu_{14}-1 is highly different from that of $Cu_{14}(C_2B_{10}H_{10}S_2)_6(CH_3CN)_8$ ($C_2B_{10}H_{10}S_2$ is 1,2-dithiolate-*o*-carborane) which features a cubic Cu_{14} core.[68] Furthermore, in sharp contrast to $[NEt_4][Cu$

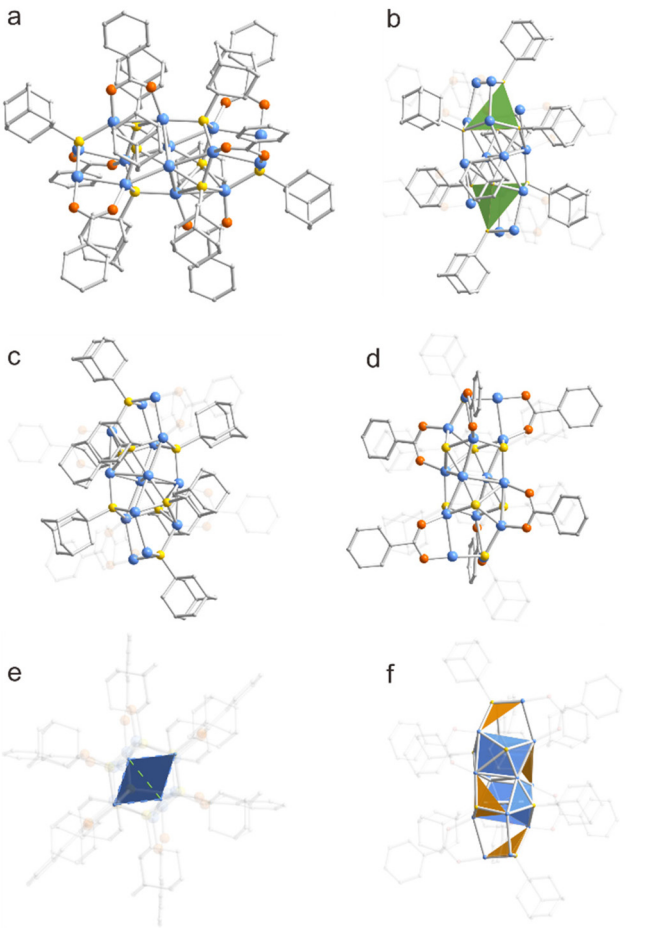

Fig. 1 (a) The total structure of the $[Cu_{14}(BEN)_6(AdmS)_8]$ cluster. (b) The tetrahedral S_4 unit in the core. (c and d) The binding pattern between the Cu atoms and ligands in the Cu_{14} metal core (one of them is highlighted). (e) Cu_4 plane at the center of the cluster. (f) Triangular conical Cu_3S (orange) and tetragonal conical Cu_4S (blue) fragment units. Color codes for atoms: blue spheres, Cu; orange spheres, O; yellow spheres, S; grey spheres, C. All hydrogen atoms are omitted for clarity.

$(AdmS)_2$] and [NEt_4][$Cu_5(AdmS)_6$], the copper atoms in the center of Cu_{14}-1 are interconnected to form a planar quadrilateral structure of Cu_4 (Fig. 1e).[56] Notably, Cu–Cu bonds (green) with 2.94 Å are found in the Cu_4 plane (Fig. 2a). The value is slightly larger than the average Cu–Cu bond lengths (Table S3†). The Cu–S–Cu bond lengths are of a wide range as well, with values between 2.138 and 2.647 Å, which is related to the two bridging modes (μ_3-S, μ_4-S) within the cluster in triangular conical Cu_3S (orange) and tetragonal conical Cu_4S (blue) fragment units, respectively (Fig. 1f). Furthermore, the Cu–S–Cu bond angles thus are in a relatively large range of 66.99–129.11°.

To confirm the formula determined by X-ray crystallographic analysis, high-resolution electrospray ionization time-of-flight mass spectroscopy (ESI-TOF-MS) of Cu_{14}-1 was then conducted in the positive mode. As shown in Fig. S5,† the ESI-MS of Cu_{14}-1 in the positive mode shows one prominent peak at ~2470 and a small peak ~3010 *m*/*z*. The two peaks can be assigned to be $[Cu_{12}(BEN)_3(AdmS)_8]^+$ and $[Cu_{15}(BEN)_6(AdmS)_8]^+$, respectively. The excellent match of the experimental and simulated isotope patterns verified the composition proposed by single crystal diffraction analysis (Fig. S5,† inset).

With Cu_{14}-1 in hand, we thus in the following section wonder whether its surface structure can be regulated by introducing different carboxylic ligands. 2-[(2,6-Dichlorophenyl) amino] benzeneacetic acid (diclofenac) was selected here considering its large steric hindrance and wide use in the area of medicine (Fig. 2). [Cu_{14}(diclofenac)$_6(AdmS)_8$] (Cu_{14}-2) can be readily obtained by a similar synthetic approach to that of Cu_{14}-1 by using diclofenac instead of BEN (Fig. S6 and S7†). It is noteworthy that Cu_{14}-2, to the best of our knowledge, represents the first copper cluster stabilized by diclofenac. Structural comparisons reveal that the metal core and coordination mode of Cu_{14}-2 are similar to those of Cu_{14}-1, with the Cu–Cu bond lengths ranging from 2.609 to 2.842 Å, Cu–O from 1.876 to 2.026 Å and Cu–S from 2.149 to 2.573 Å, respectively. Careful comparison reveals that the average Cu–Cu bond lengths in Cu_{14}-2 are slightly shorter than those of Cu_{14}-1 (Table S3†). Notably, the angles of the Cu_4 plane are highly different for the two clusters. The angle of quadrilateral in Cu_{14}-1 is 77.1°, while it is only 75.4° for Cu_{14}-2 (Fig. 2).

Despite the small structural deviations induced by using different carboxylic ligands, the physicochemical properties of the two Cu_{14} clusters are highly different. As shown in Fig. 3 (red trace), the room temperature ultraviolet-visible spectrum (UV-vis) of Cu_{14}-1 manifests a unique electronic structure, with characteristic peaks at ~235, ~275 and ~330 nm, respectively. To our surprise, the UV-Vis spectrum of Cu_{14}-2 is extremely distinct from that of Cu_{14}-1, which displays several prominent absorption bands at around 270, 350 and 500 nm, respectively (Fig. 3, green trace). We note that the heavy dependence of the optical properties on the surface ligands of Cu_{14} may facilitate their application in optics down to the nanometer scale.

To understand why the two clusters exhibit significantly different spectral properties, we have thus performed density functional theory (DFT) calculation to investigate their electronic structures. The experimental structures of the clusters were directly employed as the moieties for calculation (see technical details in the Experimental section). The simulated spectra of the two clusters, as shown in Fig. 3 (inset), exhibit similar profiles to the experimental ones. The calculated UV-Vis spectrum of Cu_{14}-1 mainly displays three absorption band wavelengths at 364, 307 and 230 nm, respectively, which

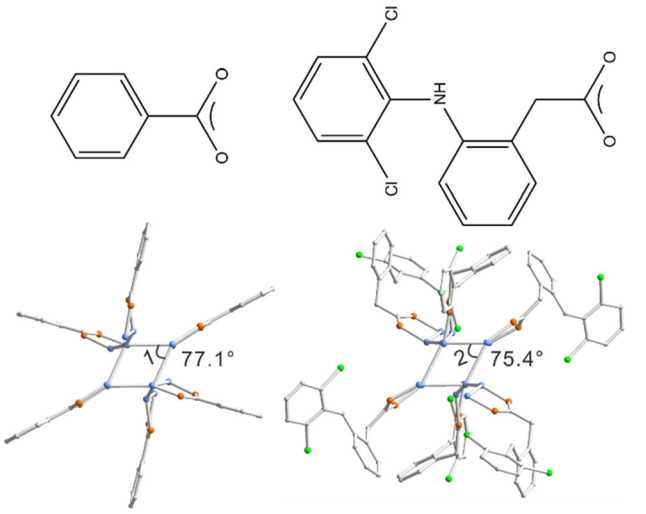

Fig. 2 Structural comparisons of Cu_{14}-1 and Cu_{14}-2 clusters stabilized by different acids. The angles of the Cu_4 plane are slightly different due to the use of different acids. Color codes for atoms: blue spheres, Cu; orange spheres, O; yellow spheres, S; grey spheres, C. All hydrogen atoms are omitted for clarity.

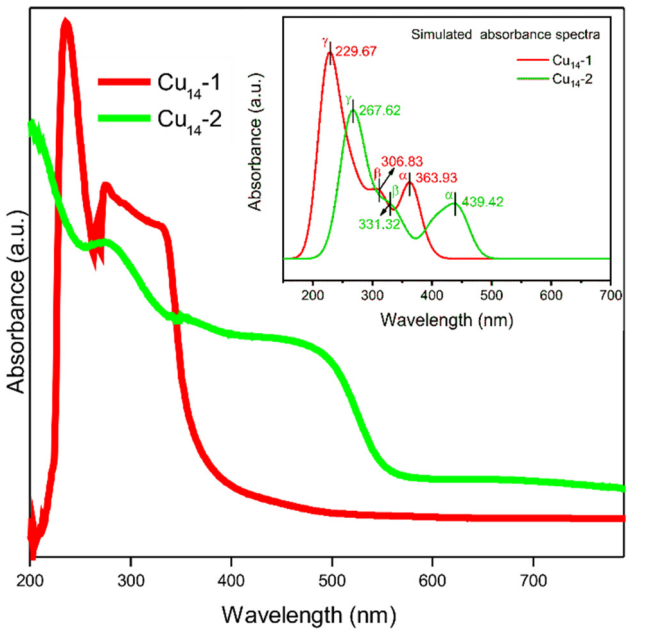

Fig. 3 Experimental UV-Vis spectra of Cu_{14}-1 and Cu_{14}-2 clusters in dichloromethane. The inset shows the simulated absorbance spectra of Cu_{14}-1 and Cu_{14}-2 clusters.

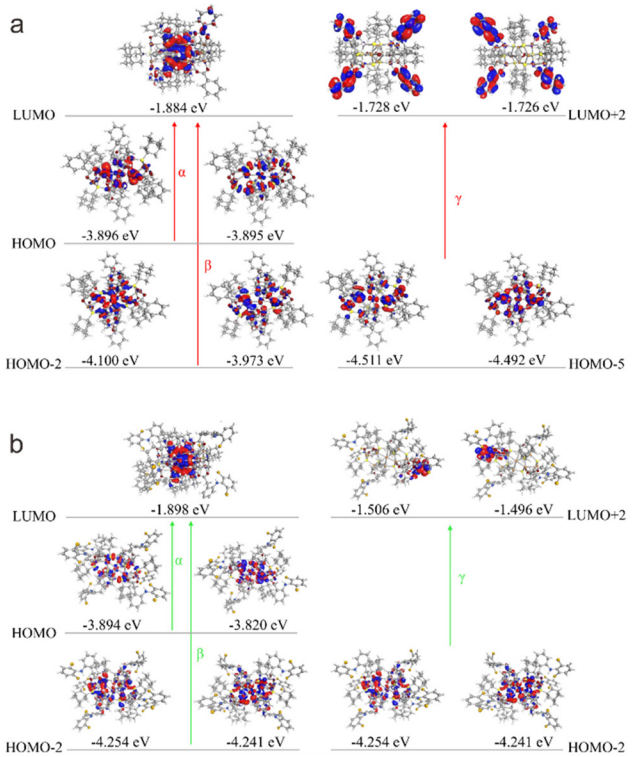

Fig. 4 Orbitals involved in the α, β and γ transitions of Cu_{14}-1 (a) and Cu_{14}-2 (b).

are attributed to the transition of α (HOMO to LUMO transition), β (HOMO−2 to LUMO) and γ (HOMO−5 to LUMO+2), respectively (Fig. 4a). As a comparison, the simulated UV spectrum of Cu_{14}-2 exhibits an electronic transition from HOMO−2 to LUMO+2 with the minimum wavelength at 268 nm (Fig. 4b). It suggests that the energy levels for the electronic transitions of the two clusters are different, therefore rationalizing their distinct optical properties.

Not only absorbance features of the two clusters have been tailored significantly by using different types of carboxylates, but also their stability and self-assembly modes. As suggested by the time-dependent UV-Vis spectra (Fig. S8†), while Cu_{14}-1 exhibits high stability in the solution form, Cu_{14}-2 is prone to decompose under similar conditions. Moreover, the two clusters are in practically different space groups ($P\bar{1}$ for Cu_{14}-1 and $P2_1c$ for Cu_{14}-2). Shown in Fig. 5 is the comparison of the assembly structures of the two clusters. The packing structure of Cu_{14}-1 is loosely arranged in the linear mode along the *c*-axis (Fig. 5a), while that of Cu_{14}-2 is in a twisted style by closely touching with each other (Fig. 5b). The distinction observed above strongly indicates the efficiency of employing different carboxylates as protective shells for regulating assembly chemistry of metal clusters.

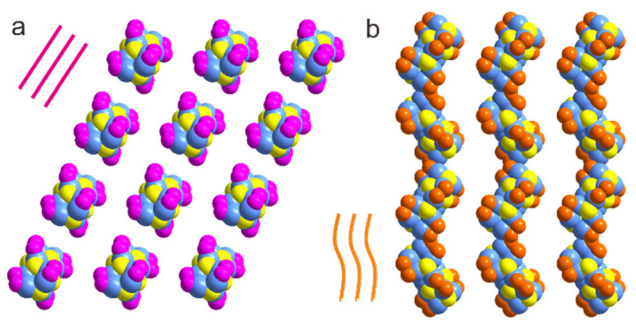

Fig. 5 Assembly structures of Cu_{14}-1 (a) and Cu_{14}-2 (b) clusters along the *c*-axis. Color codes for atoms: blue spheres, Cu; magenta and orange spheres, O; yellow spheres, S. All other atoms are omitted for clarity.

Conclusions

In summary, we report the synthesis and structural determination of two novel copper nanoclusters stabilized by carboxylate ligands, which motivates the wide exploration of carboxylates as the next generation of surface ligands for the protection of metal nanoclusters. We have also introduced, for the first time, diclofenac as a ligand for the stabilization of copper clusters, implying their potential applications in medicine. Moreover, it has been demonstrated that the metal skeleton, surface structure, optical properties, stability, and assembly structures of carboxylic-protected metal nanoclusters can be tuned by employing different carboxylic groups. These Cu_{14} clusters reported herein not only have application prospects in the fields of optics and catalysis, but also can be regarded as a model system to study the fundamental issue of structure–activity relationship. More studies on preparing carboxylate-functionalized metal nanoclusters are ongoing in our laboratories to deepen the understanding of metal–carboxylic interfaces and the relationship between their structures and performances.

Experimental

Materials

Copper sulfate ($CuSO_4$, 99%), 2-[(2,6-dichlorophenyl) amino] benzeneacetic acid (diclofenac, 98%), benzoic acid (C_6H_5COOH, 98%) and 1-adamantanethiol (AdmSH, 98%) were purchased from Bidepharm (Shanghai, China). Dichloromethane (CH_2Cl_2, A.R.), ethylene glycol ($(CH_2OH)_2$, A.R.), toluene (C_7H_8, A.R.) and ether ($C_4H_{10}O$, A.R.) were purchased from Sinopharm Chemical Reagent Co. Ltd (Shanghai, China). Water used in all experiments was ultrapure. All other reagents were used as received without further purification.

Synthesis of $Cu(C_6H_5COO)_2$ and Cu(diclofenac)$_2$

$Cu(C_6H_5COO)_2$ was synthesized by dissolving 28.8 mg of C_6H_5COONa and 16 mg of $CuSO_4$ in 10 mL of deionized water. After stirring for 2 h at room temperature, the reaction mixture was filtered, and the green precipitate was washed with water and dried in air. The resulting copper salts were obtained in

good yield. Cu(diclofenac)$_2$ was prepared using a similar procedure except for the use of 32 mg of Na(diclofenac) and 16 mg of $CuSO_4$ as precursors.

Synthesis of Cu_{14}

Cu_{14}-1 was prepared by a modified procedure of copper-based metal–organic chalcogenides. Typically, $Cu(C_6H_5COO)_2$ and AdmSH at a molar ratio of 1 : 1 were dissolved in a mixed solvent of ethylene glycol and toluene. The mixture was heated at 80 °C over a period of 48 h, resulting in a yellow solution. The solution was then carefully filtered and dried up. To the solid, dichloromethane was added, affording a yellow solution. Yellow block crystals were obtained by vapor diffusion of ether into the solution. Cu_{14}-2 was prepared by a similar procedure of Cu_{14}-1, except for the use of Cu(diclofenac)$_2$ instead of $Cu(C_6H_5COO)_2$.

Characterization studies

UV-Vis spectra. UV-Vis spectra were collected using a Carry-5000 Spectrophotometer using a quartz cuvette of 1 cm path length. The scanning speed was 1000 nm min^{-1}. The spectra were recorded in diluted solutions of dichloromethane and the signal of the blank solvent was subtracted.

ESI-MS. Electrospray ionization mass spectra (ESI-MS) were recorded using an Agilent 6224 time-of-flight mass spectrometer in the positive mode. The samples dissolved in dichloromethane were filtered before the measurements. Then the sample was directly infused at a flow rate of 1.2 mL h^{-1} using a syringe pump. Typical parameters used for the measurements were as follows: capillary voltage: 4.0 kV; drying gas temp.: 150 °C; drying gas flow: 4 L min^{-1}; nebulizer pressure: 20 psi.

Crystallography. X-ray single-crystal analysis: the diffraction data of the single crystals of compounds Cu_{14}-1 and Cu_{14}-2 were collected using a Rigaku Oxford Diffraction system X-ray single-crystal diffractometer using Cu Kα (λ = 1.54184 Å) at 293 K. The data were processed using CrysAlis^{Pro}. The structure was solved and refined using full-matrix least-squares based on F_2 using ShelXT,[69] ShelXL[70] in Olex2,[71] and Shelxle.[72] The thermal ellipsoids of the ORTEP diagram were generated at 50% probability. Detailed crystal data and structural refinements for the two compounds are given in Tables S1 and S2.† CCDC 2216708 and 2216705† contain the supplementary crystallographic data for this paper.

Computational details

As for the optical-absorption spectrum and orbital information, the density functional theory (DFT) calculations were implemented in the quantum chemistry program Turbomole V4.2.[73] Geometry optimization of the two Cu_{14} clusters was carried out by DFT calculations with the TPSS (Tao, Perdew, Staroverov, and Scuseria) functional for electron exchange and correlation and def2-SV(P) for orbital and auxiliary basis sets.[74] Of note, the def2-SV(P) basis sets were used for S, N, O, Cl, C and H, while effective core potentials which include scalar relativistic corrections were considered for Cu.[75,76] Then, the time-dependent DFT computation of the optical absorption spectrum was performed at the PBE level with the def2-SV(P) basis sets. All transitions together with their oscillator strengths were then convoluted with a Gaussian line shape of 0.5 eV broadening to generate the optical-absorption spectrum.

Author contributions

The manuscript was written through contributions of all authors. H. S., Q. T. and Chaolumen supervised the project. J. S., F. S., J. T. and X. T. prepared the cluster samples and conducted the characterization studies. Q. W., R. H., A. H., Sachurilatu and X. S. were responsible for analyzing the data. All authors contributed to composing the manuscript.

Conflicts of interest

There are no conflicts to declare.

Acknowledgements

We are grateful for the financial support provided by the NSFC (2022161035), the Inner Mongolia Autonomous Region Fund for Natural Science (2021MS02001), and the Education Department of Inner Mongolia Autonomous Region (NJYT22089).

References

1 R. Jin, C. Zeng, M. Zhou and Y. Chen, Atomically Precise Colloidal Metal Nanoclusters and Nanoparticles: Fundamentals and Opportunities, *Chem. Rev.*, 2016, **116**, 10346.
2 Y. Du, H. Sheng, D. Astruc and M. Zhu, Atomically Precise Noble Metal Nanoclusters as Efficient Catalysts: A Bridge between Structure and Properties, *Chem. Rev.*, 2020, **120**, 526.
3 X. Liu and D. Astruc, Atomically precise copper nanoclusters and their applications, *Coord. Chem. Rev.*, 2018, **359**, 112.
4 A. J. Jordan, G. Lalic and J. P. Sadighi, Coinage Metal Hydrides: Synthesis, Characterization, and Reactivity, *Chem. Rev.*, 2016, **116**, 8318.
5 Z. Gan, N. Xia and Z. Wu, Discovery, Mechanism, and Application of Antigalvanic Reaction, *Acc. Chem. Res.*, 2018, **51**, 2774.
6 K. Konishi, M. Iwasaki and Y. Shichibu, Phosphine-Ligated Gold Clusters with Core + exo Geometries: Unique Properties and Interactions at the Ligand-Cluster Interface, *Acc. Chem. Res.*, 2018, **51**, 3125.
7 S. Sharma, K. K. Chakrahari, J. Saillard and C. W. Liu, Structurally Precise Dichalcogenolate-Protected Copper and

Silver Superatomic Nanoclusters and Their Alloys, *Acc. Chem. Res.*, 2018, **51**, 2475.
8 R. S. Dhayal, W. E. van Zyl and C. W. Liu, Polyhydrido Copper Clusters: Synthetic Advances, Structural Diversity, and Nanocluster-to-Nanoparticle Conversion, *Acc. Chem. Res.*, 2016, **49**, 86.
9 A. Ghosh, O. F. Mohammed and O. M. Bakr, Atomic-Level Doping of Metal Clusters, *Acc. Chem. Res.*, 2018, **51**, 3094.
10 R. Jin, Y. Pei and T. Tsukuda, Controlling Nanoparticles with Atomic Precision, *Acc. Chem. Res.*, 2019, **52**, 1.
11 Z. Lei, X. K. Wan, S. F. Yuan, Z. J. Guan and Q. M. Wang, Alkynyl Approach toward the Protection of Metal Nanoclusters, *Acc. Chem. Res.*, 2018, **51**, 2465.
12 Q. Yao, T. Chen, X. Yuan and J. Xie, Toward Total Synthesis of Thiolate-Protected Metal Nanoclusters, *Acc. Chem. Res.*, 2018, **51**, 1338.
13 A. Baghdasaryan and T. Bürgi, Copper nanoclusters: designed synthesis, structural diversity, and multiplatform applications, *Nanoscale*, 2021, **13**, 6283.
14 H. Häkkinen, The gold–sulfur interface at the nanoscale, *Nat. Chem.*, 2012, **4**, 443.
15 P. D. Jadzinsky, G. Calero, C. J. Ackerson, D. A. Bushnell and R. D. Kornberg, Structure of a Thiol Monolayer-Protected Gold Nanoparticle at 1.1 Å Resolution, *Science*, 2007, **318**, 430.
16 C. Zeng, Y. Chen, K. Kirschbaum, K. J. Lambright and R. Jin, Emergence of hierarchical structural complexities in nanoparticles and their assembly, *Science*, 2016, **354**, 1580.
17 J. Yan, B. K. Teo and N. F. Zheng, Surface Chemistry of Atomically Precise Coinage-Metal Nanoclusters: From Structural Control to Surface Reactivity and Catalysis, *Acc. Chem. Res.*, 2018, **51**, 3084.
18 S. Bera, B. Xue, P. Rehak, G. Jacoby, W. Ji, L. J. W. Shimon, R. Beck, P. Kral, Y. Cao and E. Gazit, Self-Assembly of Aromatic Amino Acid Enantiomers into Supramolecular Materials of High Rigidity, *ACS Nano*, 2020, **14**, 1694.
19 P. N. Gunawardene, J. Martin, J. M. Wong, Z. Ding, J. F. Corrigan and M. S. Workentin, Controlling the Structure, Properties and Surface Reactivity of Clickable Azide-Functionalized $Au_{25}(SR)_{18}$ Nanocluster Platforms Through Regioisomeric Ligand Modifications, *Angew. Chem., Int. Ed.*, 2022, **61**, e202205194.
20 H. Shen, G. Deng, S. Kaappa, T. Tan, Y. Z. Han, S. Malola, S. C. Lin, B. K. Teo, H. Häkkinen and N. F. Zheng, Highly Robust but Surface-Active: An N-Heterocyclic Carbene-Stabilized Au_{25} Nanocluster, *Angew. Chem., Int. Ed.*, 2019, **58**, 17731.
21 H. Shen, Z. Xu, M. S. A. Hazer, Q. Wu, J. Peng, R. Qin, S. Malola, B. K. Teo, H. Häkkinen and N. F. Zheng, Surface Coordination of Multiple Ligands Endows N-Heterocyclic Carbene-Stabilized Gold Nanoclusters with High Robustness and Surface Reactivity, *Angew. Chem., Int. Ed.*, 2021, **60**, 3752.
22 X. Du and R. Jin, Atomic-precision engineering of metal nanoclusters, *Dalton Trans.*, 2020, **49**, 10701.
23 L. Xu, Q. Li, T. Li, J. Chai, S. Yang and M. Zhu, Construction of a new $Au_{27}Cd_1(SAdm)_{14}(DPPF)Cl$ nanocluster by surface engineering and insight into its structure–property correlation, *Inorg. Chem. Front.*, 2021, **8**, 4820.
24 C. Dong, R. Huang, C. Chen, J. Chen, S. Nematulloev, X. Guo, A. Ghosh, B. Alamer, M. N. Hedhili, T. T. Isimjan, Y. Han, O. F. Mohammed and O. M. Bakr, $[Cu_{36}H_{10}(PET)_{24}(PPh_3)_6Cl_2]$ Reveals Surface Vacancy Defects in Ligand-Stabilized Metal Nanoclusters, *J. Am. Chem. Soc.*, 2021, **143**, 11026.
25 P. Liu, R. Qin, G. Fu and N. F. Zheng, Surface Coordination Chemistry of Metal Nanomaterials, *J. Am. Chem. Soc.*, 2017, **139**, 2122.
26 X. Lin, C. Liu, K. Sun, R. Wu, X. Fu and J. Huang, Structural isomer and high-yield of Pt_1Ag_{28} nanocluster via one-pot chemical wet method, *Nano Res.*, 2019, **12**, 309.
27 C. Sun, N. Mammen, S. Kaappa, P. Yuan, G. Deng, C. Zhao, J. Yan, S. Malola, K. Honkala, H. Häkkinen, B. K. Teo and N. F. Zheng, Atomically Precise, Thiolated Copper–Hydride Nanoclusters as Single-Site Hydrogenation Catalysts for Ketones in Mild Conditions, *ACS Nano*, 2019, **13**, 5975.
28 Y. Cao, V. Fung, Q. Yao, T. Chen, S. Q. Zang, D. Jiang and J. Xie, Control of single-ligand chemistry on thiolated Au_{25} nanoclusters, *Nat. Commun.*, 2020, **11**, 5498.
29 H. Yang, Y. Wang, H. Huang, L. Gell, L. Lehtovaara, S. Malola, H. Hakkinen and N. F. Zheng, All-thiol-stabilized Ag_{44} and $Au_{12}Ag_{32}$ nanoparticles with single-crystal structures, *Nat. Commun.*, 2013, **4**, 2422.
30 H. Shen and T. Mizuta, An Atomically Precise Alkynyl-Protected $PtAg_{42}$ Superatom Nanocluster and Its Structural Implications, *Chem. – Asian J.*, 2017, **12**, 2904.
31 L. Jin, D. S. Weinberger, M. Melaimi, C. E. Moore, A. L. Rheingold and G. Bertrand, Trinuclear gold clusters supported by cyclic (alkyl)(amino)carbene ligands: mimics for gold heterogeneous catalysts, *Angew. Chem., Int. Ed.*, 2014, **53**, 9059.
32 H. Shen, Q. Wu, M. Asre Hazer, X. Tang, Y. Han, R. Qin, C. Ma, S. Malola, B. K. Teo, H. Häkkinen and N. F. Zheng, Regioselective hydrogenation of alkenes over atomically dispersed Pd sites on NHC-stabilized bimetallic nanoclusters, *Chem*, 2022, **8**, 2380.
33 V. K. Kulkarni, B. N. Khiarak, S. Takano, S. Malola, E. L. Albright, T. I. Levchenko, M. D. Aloisio, C. T. Dinh, T. Tsukuda, H. Häkkinen and C. M. Crudden, N-Heterocyclic, Carbene-Stabilized Hydrido Au_{24} Nanoclusters: Synthesis, Structure, and Electrocatalytic Reduction of CO_2, *J. Am. Chem. Soc.*, 2022, **144**, 9000.
34 M. R. Narouz, S. Takano, P. A. Lummis, T. I. Levchenko, A. Nazemi, S. Kaappa, S. Malola, G. Yousefalizadeh, L. A. Calhoun, K. G. Stamplecoskie, H. Hakkinen, T. Tsukuda and C. M. Crudden, Robust, Highly Luminescent Au_{13} Superatoms Protected by N-Heterocyclic Carbenes, *J. Am. Chem. Soc.*, 2019, **141**, 14997.
35 H. Shen, Q. Wu, S. Malola, Y. Han, Z. Xu, R. Qin, X. Tang, Y. Chen, B. K. Teo, H. Häkkinen and N. F. Zheng,

N-Heterocyclic, Carbene-Stabilized Gold Nanoclusters with Organometallic Motifs for Promoting Catalysis, *J. Am. Chem. Soc.*, 2022, **144**, 10844.

36 H. Shen, L. Wang, O. López-Estrada, C. Hu, Q. Wu, D. Cao, S. Malola, B. K. Teo, H. Häkkinen and N. F. Zheng, Copper-hydride nanoclusters with enhanced stability by N-heterocyclic carbenes, *Nano Res.*, 2021, **14**, 3303.

37 H. Shen, S. Xiang, Z. Xu, C. Liu, X. Li, C. Sun, S. Lin, B. K. Teo and N. F. Zheng, Superatomic Au_{13} clusters ligated by different N-heterocyclic carbenes and their ligand-dependent catalysis, photoluminescence, and proton sensitivity, *Nano Res.*, 2020, **13**, 1908.

38 M. R. Narouz, K. M. Osten, P. J. Unsworth, R. W. Y. Man, K. Salorinne, S. Takano, R. Tomihara, S. Kaappa, S. Malola, C. T. Dinh, J. D. Padmos, K. Ayoo, P. J. Garrett, M. Nambo, J. H. Horton, E. H. Sargent, H. Häkkinen, T. Tsukuda and C. M. Crudden, N-heterocyclic carbene-functionalized magic-number gold nanoclusters, *Nat. Chem.*, 2019, **11**, 419.

39 H. Shen, Y. Han, Q. Wu, J. Peng, B. K. Teo and N. F. Zheng, Simple and Selective Synthesis of Copper–Containing Metal Nanoclusters Using $(PPh_3)_2CuBH_4$ as Reducing Agent, *Small Methods*, 2020, **5**, 2000603.

40 C. Liu, S. F. Yuan, S. Wang, Z. J. Guan, D. Jiang and Q. M. Wang, Structural transformation and catalytic hydrogenation activity of amidinate-protected copper hydride clusters, *Nat. Commun.*, 2022, **13**, 2082.

41 T. Chiu, J. Liao, F. Gam, Y. Wu, X. Wang, S. Kahlal, J. Saillard and C. W. Liu, Hydride-Containing Eight-Electron Pt/Ag Superatoms: Structure, Bonding, and Multi-NMR Studies, *J. Am. Chem. Soc.*, 2022, **144**, 10599.

42 L. G. AbdulHalim, M. S. Bootharaju, Q. Tang, S. Del Gobbo, R. G. AbdulHalim, M. Eddaoudi, D. Jiang and O. M. Bakr, $Ag_{29}(BDT)_{12}(TPP)_4$: A Tetravalent Nanocluster, *J. Am. Chem. Soc.*, 2015, **137**, 11970.

43 R. S. Dhayal, J. Liao, S. Kahlal, X. Wang, Y. Liu, M. Chiang, W. E. van Zyl, J. Saillard and C. W. Liu, $[Cu_{32}(H)_{20}\{S_2P(O^iPr)_2\}_{12}]$: The Largest Number of Hydrides Recorded in a Molecular Nanocluster by Neutron Diffraction, *Chem. – Eur. J.*, 2015, **21**, 8369.

44 Z. Wang, H. Su, L. Zhang, J. Dou, C. H. Tung, D. Sun and L. Zheng, Stepwise Assembly of Ag_{42} Nanocalices Based on a MoVI-Anchored Thiacalix[4]arene Metalloligand, *ACS Nano*, 2022, **16**, 4500.

45 A. Ghosh, R. W. Huang, B. Alamer, E. Abou-Hamad, M. N. Hedhili, O. F. Mohammed and O. M. Bakr, $[Cu_{61}(S^tBu)_{26}S_6Cl_6H_{14}]^+$: A Core–Shell Superatom Nanocluster with a Quasi-J_{36} Cu_{19} Core and an "18-Crown-6" Metal-Sulfide-like Stabilizing Belt, *ACS Mater. Lett.*, 2019, **1**, 297.

46 C. Li, J. Zhao, L. Xie, J. Wu, Q. Ren, Y. Wang and G. Li, Surface-Adsorbed Carboxylate Ligands on Layered Double Hydroxides/Metal-Organic Frameworks Promote the Electrocatalytic Oxygen Evolution Reaction, *Angew. Chem., Int. Ed.*, 2021, **60**, 18129.

47 Y. Liu, X. Xi, C. Ye, T. Gong, Z. Yang and Y. Cui, Chiral metal-organic frameworks bearing free carboxylic acids for organocatalyst encapsulation, *Angew. Chem., Int. Ed.*, 2014, **53**, 13821.

48 C. A. Salazar, J. J. Gair, K. N. Flesch, I. A. Guzei, J. C. Lewis and S. S. Stahl, Catalytic Behavior of Mono-N-Protected Amino-Acid Ligands in Ligand-Accelerated C-H Activation by Palladium(II), *Angew. Chem., Int. Ed.*, 2020, **59**, 10873.

49 O. Karagiaridi, N. A. Vermeulen, R. C. Klet, T. C. Wang, P. Z. Moghadam, S. S. Al-Juaid, J. F. Stoddart, J. T. Hupp and O. K. Farha, Functionalized defects through solvent-assisted linker exchange: synthesis, characterization, and partial postsynthesis elaboration of a metal-organic framework containing free carboxylic acid moieties, *Inorg. Chem.*, 2015, **54**, 1785.

50 X. Lv, L. Feng, L. Xie, T. He, W. Wu, K. Wang, G. Si, B. Wang, J. Li and H. Zhou, Linker Desymmetrization: Access to a Series of Rare-Earth Tetracarboxylate Frameworks with Eight-Connected Hexanuclear Nodes, *J. Am. Chem. Soc.*, 2021, **143**, 2784.

51 T. Zhou, P. F. Qian, J. Y. Li, Y. B. Zhou, H. C. Li, H. Y. Chen and B. F. Shi, Efficient Synthesis of Sulfur-Stereogenic Sulfoximines via Ru(II)-Catalyzed Enantioselective C-H Functionalization Enabled by Chiral Carboxylic Acid, *J. Am. Chem. Soc.*, 2021, **143**, 6810.

52 Z. Xue, K. Liu, Q. Liu, Y. Li, M. Li, C. Su, N. Ogiwara, H. Kobayashi, H. Kitagawa, M. Liu and G. Li, Missing-linker metal-organic frameworks for oxygen evolution reaction, *Nat. Commun.*, 2019, **10**, 5048.

53 J. Zhang, L. D. Ellis, B. Wang, M. J. Dzara, C. Sievers, S. Pylypenko, E. Nikolla and J. W. Medlin, Control of interfacial acid–metal catalysis with organic monolayers, *Nat. Catal.*, 2018, **1**, 148.

54 R. E. Plata, D. E. Hill, B. E. Haines, D. G. Musaev, L. Chu, D. P. Hickey, M. S. Sigman, J. Q. Yu and D. G. Blackmond, A Role for Pd(IV) in Catalytic Enantioselective C-H Functionalization with Monoprotected Amino Acid Ligands under Mild Conditions, *J. Am. Chem. Soc.*, 2017, **139**, 9238.

55 P. Su, Z. Zhu, Q. Fan, J. Cao, Y. Wang, X. Yang, B. Cheng, W. Liu and Y. Tang, Surface ligand coordination induced self-assembly of a nanohybrid for efficient photodynamic therapy and imaging, *Inorg. Chem. Front.*, 2018, **5**, 2620.

56 F. Kiyoshi, I. Sadako, K. Nobumasa and M. Yoshihiko, Preparation, Spectroscopic Characterization, and Molecular Structure of Copper(I) Aliphatic Thiolate Complexes, *Inorg. Chem.*, 1998, **37**, 168.

57 J. Wang, H. Liu, Z. Tong and C. Ha, Fluorescent/luminescent detection of natural amino acids by organometallic systems, *Coord. Chem. Rev.*, 2015, **303**, 139.

58 E. Shin, J. Yoo, G. Yoo, Y. Kim and Y. S. Kim, Eco-friendly cross-linked polymeric dielectric material based on natural tannic acid, *Chem. Eng. J.*, 2019, **358**, 170.

59 X. Zhao, E. T. Nguyen, A. N. Hong, P. Feng and X. Bu, Chiral Isocamphoric Acid: Founding a Large Family of Homochiral Porous Materials, *Angew. Chem., Int. Ed.*, 2018, **57**, 7101.

60 B. Han, Z. Liu, L. Feng, Z. Wang, R. K. Gupta, C. M. Aikens, C. H. Tung and D. Sun, Polymorphism in Atomically

Precise Cu_{23} Nanocluster Incorporating Tetrahedral $[Cu_4]^0$ Kernel, *J. Am. Chem. Soc.*, 2020, **142**, 5834.

61 A. W. Cook, Z. R. Jones, G. Wu, S. L. Scott and T. W. Hayton, An Organometallic Cu_{20} Nanocluster: Synthesis, Characterization, Immobilization on Silica, and "Click" Chemistry, *J. Am. Chem. Soc.*, 2018, **140**, 394.

62 X. M. Luo, C. H. Gong, X. Y. Dong, L. Zhang and S. Q. Zang, Evolution of all-carboxylate-protected superatomic Ag clusters confined in Ti-organic cages, *Nano Res.*, 2021, **14**, 2309.

63 T. Liu and D. Jiang, Understanding the interaction between carboxylates and coinage metals from first principles, *J. Chem. Phys.*, 2021, **155**, 034301.

64 K. G. Liu, X. M. Gao, T. Liu, M. L. Hu and D. E. Jiang, All-Carboxylate-Protected Superatomic Silver Nanocluster with an Unprecedented Rhombohedral Ag_8 Core, *J. Am. Chem. Soc.*, 2020, **142**, 16905.

65 W. D. Liu, J. Q. Wang, S. F. Yuan, X. Chen and Q. M. Wang, Chiral Superatomic Nanoclusters Ag_{47} Induced by the Ligation of Amino Acids, *Angew. Chem., Int. Ed.*, 2021, **60**, 11430.

66 H. Yan, J. N. Hohman, F. H. Li, C. Jia, D. Solis-Ibarra, B. Wu, J. E. Dahl, R. M. Carlson, B. A. Tkachenko, A. A. Fokin, P. R. Schreiner, A. Vailionis, T. R. Kim, T. P. Devereaux, Z. X. Shen and N. A. Melosh, Hybrid metal-organic chalcogenide nanowires with electrically conductive inorganic core through diamondoid-directed assembly, *Nat. Mater.*, 2017, **16**, 349.

67 L. Asgharnejad, A. Abbasi, M. Najafi and J. Janczak, One-, two- and three-dimensional coordination polymers based on copper paddle-wheel SBUs as selective catalysts for benzyl alcohol oxidation, *J. Solid State Chem.*, 2019, **277**, 187.

68 Y. L. Li, J. Wang, P. Luo, X. H. Ma, X. Y. Dong, Z. Y. Wang, C. X. Du, S. Q. Zang and T. C. W. Mak, Cu_{14} Cluster with Partial Cu(0) Character: Difference in Electronic Structure from Isostructural Silver Analog, *Adv. Sci.*, 2019, **6**, 1900833.

69 G. M. Sheldrick, SHELXT-integrated space-group and crystal-structure determination, *Acta Crystallogr., Sect. A: Found. Adv.*, 2015, **71**, 3.

70 G. M. Sheldrick, A short history of SHELX, *Acta Crystallogr., Sect. A: Found. Crystallogr.*, 2008, **64**, 112.

71 O. V. Dolomanov, L. J. Bourhis, R. J. Gildea, J. A. K. Howard and H. Puschmann, OLEX2: a complete structure solution, refinement and analysis program, *J. Appl. Crystallogr.*, 2009, **42**, 339.

72 C. B. Hubschle, G. M. Sheldrick and B. Dittrich, ShelXle: a Qt graphical user interface for SHELXL, *J. Appl. Crystallogr.*, 2011, **44**, 1281.

73 R. Ahlrichs, M. Bär, M. Häser, H. Horn and C. Kölmel, Electronic structure calculations on workstation computers: The program system turbomole, *Chem. Phys. Lett.*, 1989, **162**, 165.

74 J. Tao, J. P. Perdew, V. N. Staroverov and G. E. Scuseria, Climbing the Density Functional Ladder: Nonempirical Meta–Generalized Gradient Approximation Designed for Molecules and Solids, *Phys. Rev. Lett.*, 2003, **91**, 146401.

75 D. Andrae, U. Häußermann, M. Dolg, H. Stoll and H. Preuß, Energy-adjustedab initio pseudopotentials for the second and third row transition elements, *Theor. Chim. Acta*, 1990, **77**, 123.

76 D. Andrae, U. Häußermann, M. Dolg, H. Stoll and H. Preuß, Energy-adjustedab initio pseudopotentials for the second and third row transition elements: Molecular test for M_2 (M=Ag, Au) and MH (M=Ru, Os), *Theor. Chim. Acta*, 1991, **78**, 247.